
Article:
Singh, H., Sreedharan, S., Oyarzabal, E. et al. (7 more authors) (2020) Mitochondriotropic lanthanide nanorods : implications for multimodal imaging. Chemical Communications, 56 (57). pp. 7945-7948. ISSN 1359-7345

https://doi.org/10.1039/d0cc02698k

Mitochondriotropic Lanthanide Nanorods: Implications for Multimodal Imaging

Harwinder Singha[a, b], Sreejesh Sreedharan[c], Esteban Oyarzabal[e], Tufan Singha Mahapatra[a], Nicola Green[d], Yen-Yu Ian Shih[e], Manasmita Das [e]*, Jim. A. Thomas[c]* , Sumit Kumar Pramanik[a]* and Amitava Das[a, b]*

[a] Central Salt and Marine Chemicals Research Institute, Bhavnagar, Gujarat, India.

[b] Academy of Scientific and Innovative Research (AcSIR), Ghaziabad- 201002, India

[c] Department of Chemistry, University of Sheffield, Western Bank, Sheffield, S3 7HF, UK

[d] Department of Biomedical Science, University of Sheffield, Western Bank, Sheffield, S3 7HF, UK

[e] Center for Animal MRI (CAMRI), University of North Carolina, Chapel Hill NC 27599

Abstract

Organelles such as mitochondria, lysosome, and nucleus, are essential for controlling basic cellular operations and metabolism. Because mitochondria play a critical role in energy production and programmed cell death, they act as prime therapeutic targets for various diseases and dysfunctional states. In this study, a multifunctional nanoplatform based on lanthanide upconverting nanorods is developed for concurrent mitochondria-targeted fluorescence imaging and preclinical MRI. This study provides critical insights into the spectral profiles of mitochondria and paves the way to developing novel, multimodal nanoprobes for mitochondria-targeted theranostics.

Mitochondria, aptly called as the "powerhouses of cell", regulate various biological processes within a cell that are crucial for its survival and functioning. Besides producing adenosine triphosphate (ATP), the "energy currency" of the cell through oxidative phosphorylation, they play a critical role in controlling the electron transport chain, cell cycle regulation, intracellular calcium signalling, cell proliferation and apoptosis.[1] Mitochondrial dysfunction has been identified as the root cause of several diseases including type 2 diabetes, cancer, diabetes and a range of age-related neurodegenerative disorders such as Parkinson's disease, Alzheimer's disease, muscular dystrophy, Lou Gehrig's disease, Huntington's disease and amyotrophic lateral sclerosis. [2-4] To develop a better understanding on the role of mitochondrial dysfunction in various diseases, as well as to control them, recent years have seen a phenomenal impetus in the development of mitochondria-targeted probes

A myriad of imaging techniques are used in current clinical practice which include but not limited to optical imaging, magnetic resonance imaging (MRI), ultrasound, single-photon emission computed tomography (SPECT) and X-ray computed tomography (CT) [2-3] . With the advent of higher resolution luminescence-based imaging techniques, there have been a recent surge in reports on various mitochondria-specific fluorescent markers. [5-8] However, one single imaging modality may not be able to provide all the information required from a single experiment. To address this limitation, multimodal imaging strategies are being developed. Using two or more imaging modalities simultaneously synergizes the strengths of individual modalities and enhances accuracy of diagnosis through cross-modality validation and direct, inter-modality comparison.[11-12] Traditionally, each imaging modality employs a different probe, which possesses a distinctive chemical composition, unique physicochemical properties and pharmacokinetic profile. For *in vivo* applications, it is difficult to implement a "cocktail approach" where a mixture of multiple probes is administered through a single dose in order to achieve spatiotemporal homogeneity between the individual imaging modalities. Therefore, a single probe that integrate the contrasting properties of two or more imaging probes into an all-in-one system are actively being sought for dedicated multimodal imaging.

Among the various imaging modalities that have become an indispensable part of modern clinical diagnostics, MRI has gained substantial importance due to its noninvasiveness, high spatial resolution, deep penetration and absence of radiation hazards. Despite these promising attributes, a major limitation of MRI is its low sensitivity [13-14]. This limitation can be circumvented by using suitable contrast agents that can enhance the image contrast between normal and diseased tissues by altering the longitudinal (T_1) and transverse (T_2) relaxation rates

of water protons surrounding the target region of interest. While MRI serves as an important diagnostic tool for high resolution anatomical and functional imaging, fluorescence-based optical imaging provides highly sensitive detection, quantification and real-time-tracking of bio-molecules of interest at the tissue, cellular and sub-cellular level.[15-16] Subsequently, bimodal contrast agents, integrating the synergistic advantages of both MRI and fluorescence-based optical imaging, have gained substantial attention in preclinical research. In this context, lanthanide-doped up-converting nanoparticles (UCNP) deserves special mention because of their unique ability to convert near infrared excitation into visible and ultraviolet emission, endowing greater tissue penetration, lower autofluorescence and reduced toxicity.[17-18] With an additional dopant like the gadolinium (Gd^{3+}) ion, which possesses intrinsic paramagnetism due to the presence of 7 unpaired electrons in its 4f shell, UCNPs can be used for simultaneous MRI and optical imaging. Furthermore, when conjugated with appropriate functional molecules (e.g. antibodies, peptides, drugs or photosensitizer), such UCNPs can serve as prospective candidates for targeted multimodal imaging and therapy.[19]

Herein, we report the development of a multifunctional nanoplatform based on $NaYF_4$:Yb,Gd,Eu upconverting nanorods (UCNR) that can be used for concurrent mitochondria-targeted fluorescence imaging and preclinical MRI. The presence of Eu^{3+} ions in the core of this nanosystem facilitates robust upconversion luminescence whereas Gd^{3+} endows MRI visibility. To further facilitate mitochondrial targeting, the as-prepared UCNRs were functionalized with triphenyl phosphonium cations, a known mitochondria targeting agent[6], through covalent bonding. Our results demonstrated that UCNRs developed in this study can be used as a safe and effective bimodal probe for mitochondrial-targeted optical imaging and dual T_1- and T_2-weighted MRI. This nanoprobe demonstrated robust T_1 contrast enhancement *in vivo* for high resolution cerebral microangiography, corroborating that the UCNRs stay in blood circulation post-injection to demonstrate measurable contrast.

$NaYF_4$:Eu,Gd,Eu UCNRs with uniform size were synthesized by a hydrothermal reaction (ESI†).[20] The crystallinity, phase purity and composition of the synthesized UCNRs were determined by powder XRD. The powder-XRD pattern of the synthesized UCNRs (Fig. S1, ESI†) exhibited sharp diffraction peaks that are indexed to pure hexagonal-phase β-NaYF4 nanocrystals (JCPDS No. 0281192; space group: P63/m).[21] Mitochondriotropic UCNRs were produced by chemical coupling of triphenyl phosphine (TPP) with amine-functionalized, silica-coated UCNRs, prepared using typical Stöber-based surface modification.[21] The ζ potentials of pristine UCNRs and amine functionalized silica-coated-UCNR were measured as

−26.7 and +34.07 mV, respectively. After reaction with TPP, the ζ potential of the UCNRs further increased to +36.4 mV. The presence of positive charges indicated that TPP-coated UCNRs possess a suitable targeting moiety for the negatively charged mitochondrial membrane. As evident from transmission electron microscopy (TEM) image, the synthesized nanoparticles were rod-shaped, had good monodispersity and possessed uniform sizes with an overall diameter of 18 ± 3 nm (Fig. 1a and Fig. S2, ESI†). The selected area electron diffraction pattern (SAED) and high-resolution TEM (HRTEM) image showed the lattice fringes with a *d* spacing of 0.30 nm, which was in good agreement with the lattice spacing of the (111) planes of hexagonal $NaGdF_4$ (Fig. 1 b-c). The energy dispersive X-ray (EDX) analysis confirmed that the synthesized UCNRs were composed of Y, F, Si, Yb, Gd and Eu (Fig. S3, ESI†). The upconversion photoluminescence properties of the UCNRs were studied by excitation with a 980 nm laser beam. As depicted in Fig. 1f, typical Eu^{3+} emissions coming from $^5D_0 \rightarrow {}^7F_1$ and $^5D_0 \rightarrow {}^7F_2$ were cantered at 590.3 and 613.3 nm, respectively.[22-24] Fourier transform infrared (FT-IR) spectroscopy was used to recognize the functional groups on the surface of the nanocomposites and provide evidence for successful modification. The FT-IR spectra of bare-UCNRs, amine functionalised Si-coated UCNRs, and TPP functionalised UCNRs are presented in Fig. 1e. The transmission bands at 2841 and 2940 cm^{-1} were assigned to the asymmetric and symmetric stretching vibrations of methylene ($-CH_2$) groups, associated with a thin layer of hypermer B246 on the surface of UCNRs. B246 is a polyhydroxystearic acid/polyethylene oxide/polyhydroxystearic acid, ABA block copolymer, used as a surfactant during the synthesis of nanocomposite. The FTIR spectra also reveal a broad band at around 3431 cm^{-1} originating from the O−H stretching vibration of the polyhydroxystearic acid block of B246. After the Stöber-based surface modification, new bands were observed at 3150 cm^{-1} (very broad) and 1596 cm^{-1}, emanating from N–H stretching and N–H bending vibrations, respectively. In addition, typical Si−O−Si deformation (632 and 451 cm^{-1}) and asymmetric stretching vibration of Si–O bond appeared at 1421 cm^{-1}. After TPP conjugation, asymmetrical deformation of P-C bonds was observed at 1445-1322 cm^{-1}, confirming successful anchorage of phosponium ions on the surface of UCNRs.

As $NaYF_4$:Yb,Gd,Eu NRs are well-established optical upconversion systems, we evaluated the suitability of this new probe for two photon microscopy (TPM) (Fig. 2). The intracellular uptake and subcellular trafficking of UCNRs were studied in a murine macrophage cell line viz. RAW 264.7. TPM images of RAW 264.7 cells revealed strong intracellular emission signals within the cytosol, confirming the cellular internalization of UCNRs Fig. 2a.

As the concentration of UCNRs was increased, an associated increase in intracellular luminescence was detected Fig. 2b. This trend was also evident in the intensity maps generated from these data Fig. 2c. The punctated nature of the images, which is detected in the intensity maps (Fig. 3c), also suggests that UCNRs localize in specific regions within the cytoplasm. To further verify whether the TPP-functionalized UCNRs developed in this study have mitochondrial targeting property, cells were stained with Mito Tracker green (MTG), a mitochondria-selective dye whose spectral properties are complementary to those of the UCNRs. Subsequently, their subcellular trafficking and compartmentalization was examined in-depth using the super-resolution structured illumination microscopy. In these experiments the nanorods were one-photon excited at 488 nm and their emission collected at 550 to 650 nm, whereas MTG was excited at 490 nm and observed to emit at 516 nm (Fig. 3). The intensity profile of the Widefield images revealed that 80 percent of the signals of MTG matches with that of the TPP-UCNRs. This observation along with the high calculated Pearson's coefficient (91%), suggests that TPP-UCNRs localize in the mitochondria of RAW cells (Fig. 3). For further validation of mitochondrial localization, similar co-localization experiments were performed with a lysosome-selective stain, Lyso Tracker Green (LTG) (Fig. S4 ESI†). Our results confirmed that TPP-UCNRs do not localise over lysosome or nuclei and are specifically targeted towards mitochondria.

To further examine if the synthesized UCNRs can be used as a contrast agent for MRI applications, *in vitro* relaxometry studies with TPP-UCNRs was performed using a custom-designed holder and the well-established, spin-echo based T_1-T_2 mapping protocol. The T_1- and T_2-weighted MRI phantom images of UCNRs in PBS acquired at different repetition time (TR) and echo time (TE) are presented in Fig. 4a. As evident from these images, the exact relationship between MR signal intensity and Gd^{3+} concentration was nonlinear and dependent on the pulse sequence parameters used during image acquisition. At lower concentrations (0-8 mM Gd^{3+}), T_1 weighting was predominant and UCNRs exhibited concentration-dependent positive contrast-enhancement when compared to saline control. In this regime, the T_1 relaxation rate increases linearly with increasing Gd^{3+} concentration (Fig. 4b) until the positive contrast reaches its maximum enhancement point, the value of which depends on the TR used as well as T_1 and T_2 relaxivity of the contrast material (Fig 4c). Beyond this maximal contrast enhancement (maxCE) point, the initially observed linear relationship between T_1 relaxation rate and Gd^{3+} concentration (Fig. 4b) becomes non-linear and the MR signal starts to diminish owing to T_2* related signal loss. The R_1 and R_2 relaxivity of UCNRs were determined to be 3.4

$mM^{-1}s^{-1}$ and 23.5 $mM^{-1}s^{-1}$ respectively (Fig. 4c). The R_1 relaxivity of UCNRs were comparable to that of literature-reported values for Gd-DOTA and Gd-DTPA at 9.4 T[25]. Although the UCNRs exhibited distinct T_2-effects at higher Gd^{3+} concentrations and longer TR and TE, its R_2/R_1 ratio (6.91) was almost 14.8 times lower than the measured R_2/R_1 value (102.6) for the well-known ultrasmall iron-oxide nanoparticle based MRI contrast agent, Ferumoxytol (Feraheme, AMAG Pharmaceuticals) under similar experimental conditions (R_1 = 1.412 $mM^{-1}s^{-1}$; R_2 = 144.9 $mM^{-1}s^{-1}$ (ESI†). These results indicate that TPP-UCNRs are more suited for T_1-weighted MRI; however, depending on the magnetic field strength, pulse-sequence, imaging parameters (e.g. TR, TE, flip angle etc.) and concentration of Gd^{3+} chosen, this nanoprobe can be used to achieve enhanced T_1 as well as tunable T_1-T_2 dual modal contrasts for MRI applications. These observations are in agreement with earlier reports[26-27].

To further explore if the synthesized UCNRs can be used as a contrast agent for *in vivo* MRI applications, we performed cerebromicroangiography in healthy C57BL/6 mice using UCNRs as the contrast agent. Of note, our *in vivo* studies were not designed for large group statistics tackling a biological question and was rather intended to establish a proof-of-concept that the nanoprobe developed in this study can stay in blood circulation to offer robust T_1 contrast enhancement *in vivo.* Fig. 5a presents the raw pre-and post-contrast MR images of a mouse brain acquired at 200μm^3 spatial resolution using a T_1-weighted FLASH-3D sequence. The post-contrast image revealed the presence of several small cerebral vessels that were not visible prior to the injection of UCNRs. Fig. 5b shows the representative 3D cerebrovasculature map of the mouse brain, presented as an overlay of the pre-contrast (white) and post-contrast (orange) images, constructed using the volume-rendering tools in Amira. We succeeded in identifying several key arteries and veins from this dataset including the superior sagittal sinus, transverse sinus, rostral rhinal vein, middle cerebral artery, internal carotid artery, anterior, posterior and superior cerebral artery and circle of Willis. These results indicate that UCNRs developed in this study can be used as a T_1-agent for micro-magnetic resonance angiography (MRA) *in vivo*, allowing improved visualization and delineation of vessels. This feature is certainly beneficial for the diagnosis of vascular malformations associated with a wide range of medical conditions including vasculopathies such as athelosclerosis, neurogenerative disorders such as Alzheimer's diseases, and neoplastic diseases e.g. glioblastoma multiferrome. Although in-depth pharmacokinetic evaluation is necessary to quantify the circulation half-life of these UCNRs, their MRI detectability in the vessels suggest that following intravenous injection, UCNRs are not immediately sequestered by the mononuclear phagocytic system and

remains in the blood pool throughout the period of data acquisition (~12 min) to demonstrate robust T_1 contrast enhancement for cerebral microangiography.

To further ensure the safety of TPP-UCNRs for biologically relevant applications, in *vitro* cellular viability studies were performed using the MTT assay. Our results indicated that the cell viability remained unaltered as compared to that of control group. Certainly, no decrease below 98% was detected even after exposures to different concentrations of phosphine conjugated UCNRs up to 48 h (Fig. S5, ESI†). These results indicate that the UCNRs are biocompatible, making them excellent candidates for biomedical applications.

In conclusion, we have developed a novel, lanthanide-based upconversion nanoplatform for simultaneous mitochondria-targeted optical imaging and T_1-T_2 dual modal MRI. Judicious integration of paramagnetic and upconversion luminescent properties on to the same platform results in a multifunctional, mitochondriotropic nanosystem that opens up new avenues for mitochondria-targeted theranostics. Our future studies will concentrate on 1) optimizing the pharmacokinetic properties of UCNRs for various preclinical imaging applications and 2) combining the current method with appropriate blood-brain-barrier opening technologies, which is crucial for UCNR-mediated MR imaging of mitochondrial function *in vivo*.

Acknowledgement: M.D. was supported by Cross-Disciplinary Fellowship from Human Frontier Science Program (HFSP). E.O. was supported by NIH T32HL069768. Y.Y.I.S. was supported by NIH R01NS091236, R01MH111429, R41MH113252, P60AA011605, U01AA020023, R01AA025582, U54HD079124, the Brain and Behavior Foundation Young Investigator Award, and the American Heart Association Scientist Development Award 15SDG23260025.

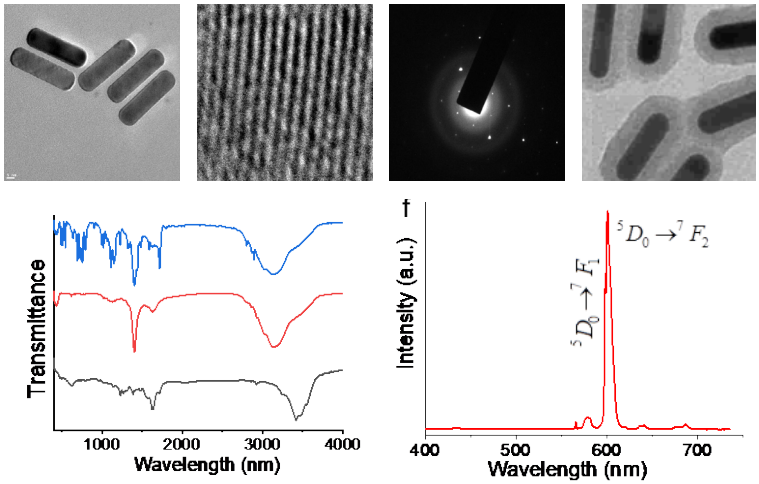

Fig. 1 TEM images of (a) β-$NaYF_4$:Yb,Gd,Eu NRs; (b) and (c) are corresponding SAED patterns and HRTEM images of b-$NaYF_4$:Yb,Gd,Eu NRs; (d) phosphine coated b-$NaYF_4$:Yb,Gd,Eu NRs;. (e) The FT-IR spectra of bare UCNRs (black); silica coated b-$NaYF_4$:Yb,Gd,Eu NRs (red) and phosphine conjugated UCNRs (blue). (f) Up conversion fluorescence spectra of solid phosphine appended $NaYF_4$:Yb,Gd,Eu NPs.

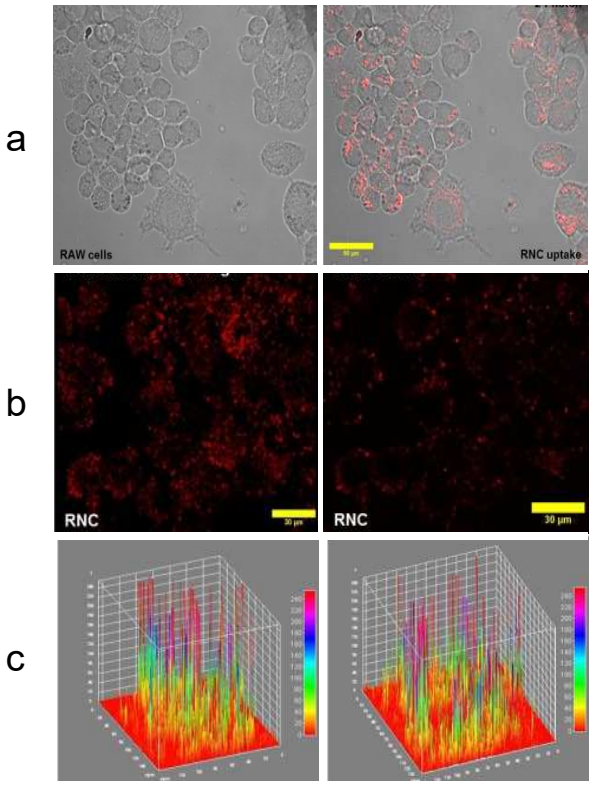

Fig. 2 Optical microscopy images showing uptake of UCNRs (a) Phase contrast (left), emission after two photon emission combined image (right) of RAW cells. (b) Effect of increasing concentration of UCP-NP treatment: 50 µg (left), 100 µg (right). (c) Intensity maps for the same concentrations shown in b. (Pseudo colour has been employed in all the images.) λ_{Ext} = 980 nm.

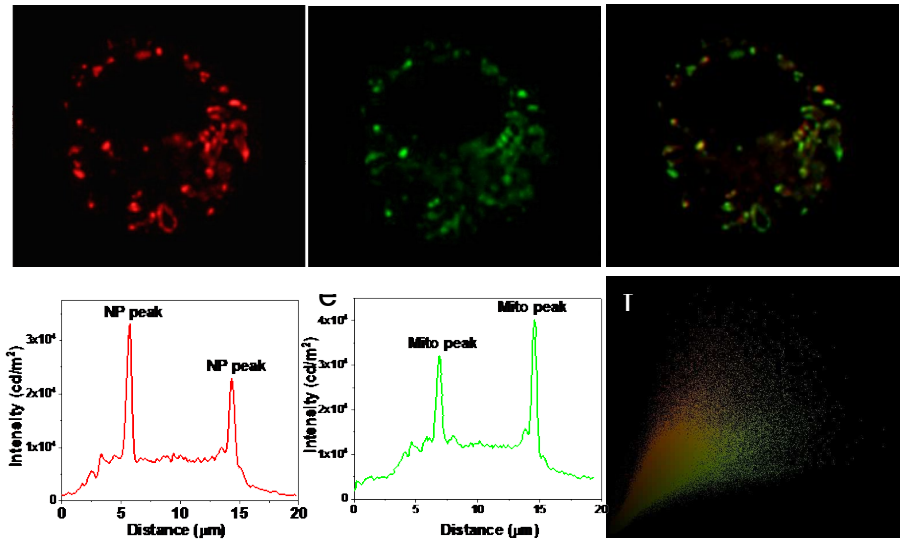

Fig. 3 Colocalization experiments (SIM Microscopy) of intracellular localization of UCNRs using mito traker probes: Wide field microscopy images of in cellulo-emission of UCNRs (panel a) with intensity along traced line shown underneath. Emission from mito traker green (panel b) and intensity along the same line shown below. The overlap of the intensity is shown in panel c. panel c shows the overlap of the green and red fluorescence, indicating mitochondrila localization of the UCNRs. Panel f shows the Pearson co-efficient = 0.92.

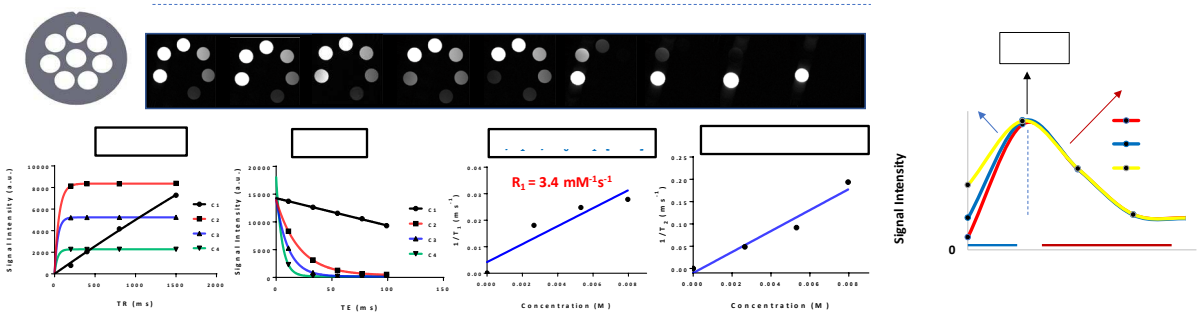

Fig. 4 In-vitro relaxometric analysis of UCNRs: (a) Representative T_1- and T_2-weighted MR phantom images of UCNRs in PBS acquired at different TR and TE; (b) Quantification of R1 and R2 from T1-recovery and T2-decay curves. (c) Effect of Gd3+ concentration on MRI signal intensity.

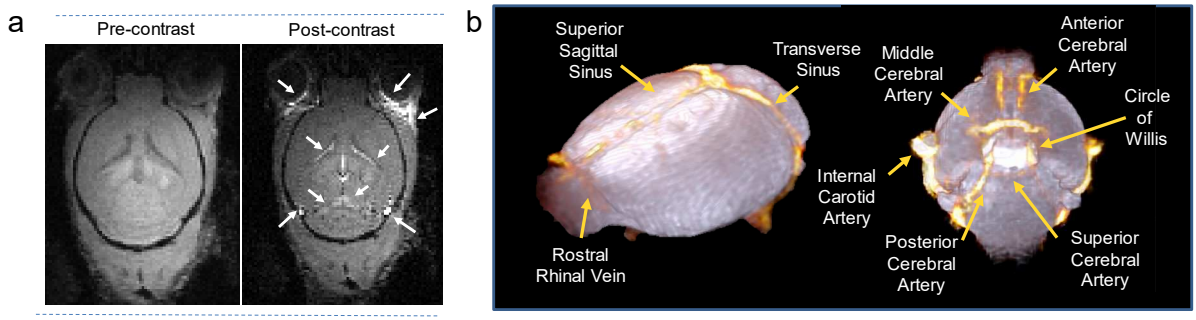

Fig. 5 (a) FLASH-3D MR images of mouse brain (axial orientation) captured at 200 μm^3 spatial resolution before and after injection of UCNRs. (b) Representative 3D cerebrovasculature map of the mouse brain generated using the volume rendering tools in Amira by overlapping the pre-contrast (in white) and post-contrast (in orange) images.

References

1. Porporato, P. E.; Filigheddu, N.; Pedro, J. M. B.-S.; Kroemer, G.; Galluzzi, L., Mitochondrial metabolism and cancer. *Cell Research* **2017,** *28*, 265.
2. Lowell, B. B.; Shulman, G. I., Mitochondrial Dysfunction and Type 2 Diabetes. *Science* **2005,** *307* (5708), 384-387.
3. Thornton, B.; Cohen, B.; Copeland, W.; Maria, B. L., Mitochondrial Disease: Clinical Aspects, Molecular Mechanisms, Translational Science, and Clinical Frontiers. *Journal of Child Neurology* **2014,** *29* (9), 1179-1207.
4. Abou-Sleiman, P. M.; Muqit, M. M. K.; Wood, N. W., Expanding insights of mitochondrial dysfunction in Parkinson's disease. *Nature Reviews Neuroscience* **2006,** *7* (3), 207-219.
5. Huang, Y.; Hu, F.; Zhao, R.; Zhang, G.; Yang, H.; Zhang, D., Tetraphenylethylene Conjugated with a Specific Peptide as a Fluorescence Turn-On Bioprobe for the Highly Specific Detection and Tracing of Tumor Markers in Live Cancer Cells. *Chemistry – A European Journal* **2014,** *20* (1), 158-164.
6. Pramanik, S. K.; Sreedharan, S.; Singh, H.; Khan, M.; Tiwari, K.; Shiras, A.; Smythe, C.; Thomas, J. A.; Das, A., Mitochondria Targeting Non-Isocyanate-Based Polyurethane Nanocapsules for Enzyme-Triggered Drug Release. *Bioconjugate Chemistry* **2018,** *29* (11), 3532-3543.
7. Leung, C. W. T.; Hong, Y.; Chen, S.; Zhao, E.; Lam, J. W. Y.; Tang, B. Z., A Photostable AIE Luminogen for Specific Mitochondrial Imaging and Tracking. *Journal of the American Chemical Society* **2013,** *135* (1), 62-65.
8. Zhao, N.; Chen, S.; Hong, Y.; Tang, B. Z., A red emitting mitochondria-targeted AIE probe as an indicator for membrane potential and mouse sperm activity. *Chemical Communications* **2015,** *51* (71), 13599-13602.
9. Huang, W.-Y.; Davis, J. J., Multimodality and nanoparticles in medical imaging. *Dalton Transactions* **2011,** *40* (23), 6087-6103.
10. Wu, M.; Shu, J., Multimodal Molecular Imaging: Current Status and Future Directions. *Contrast media & molecular imaging* **2018,** *2018*, 1382183-1382183.
11. Fjell, A. M.; Walhovd, K. B.; Brown, T. T.; Kuperman, J. M.; Chung, Y.; Hagler, D. J.; Venkatraman, V.; Roddey, J. C.; Erhart, M.; McCabe, C.; Akshoomoff, N.; Amaral, D. G.; Bloss, C. S.; Libiger, O.; Darst, B. F.; Schork, N. J.; Casey, B. J.; Chang, L.; Ernst, T. M.; Gruen, J. R.; Kaufmann, W. E.; Kenet, T.; Frazier, J.; Murray, S. S.; Sowell, E. R.; van Zijl, P.; Mostofsky, S.; Jernigan, T. L.; Dale, A. M., Multimodal imaging of the self-regulating developing brain. *Proceedings of the National Academy of Sciences* **2012,** *109* (48), 19620-19625.

12. Yang, D.; Dai, Y.; Liu, J.; Zhou, Y.; Chen, Y.; Li, C.; Ma, P. a.; Lin, J., Ultra-small BaGdF5-based upconversion nanoparticles as drug carriers and multimodal imaging probes. *Biomaterials* **2014,** *35* (6), 2011-2023.
13. Colombo, M.; Carregal-Romero, S.; Casula, M. F.; Gutiérrez, L.; Morales, M. P.; Böhm, I. B.; Heverhagen, J. T.; Prosperi, D.; Parak, W. J., Biological applications of magnetic nanoparticles. *Chemical Society Reviews* **2012,** *41* (11), 4306-4334.
14. Peng, E.; Wang, F.; Xue, J. M., Nanostructured magnetic nanocomposites as MRI contrast agents. *Journal of Materials Chemistry B* **2015,** *3* (11), 2241-2276.
15. Zhu, H.; Fan, J.; Du, J.; Peng, X., Fluorescent Probes for Sensing and Imaging within Specific Cellular Organelles. *Accounts of Chemical Research* **2016,** *49* (10), 2115-2126.
16. Xu, Z.; Xu, L., Fluorescent probes for the selective detection of chemical species inside mitochondria. *Chemical Communications* **2016,** *52* (6), 1094-1119.
17. Prodi, L.; Rampazzo, E.; Rastrelli, F.; Speghini, A.; Zaccheroni, N., Imaging agents based on lanthanide doped nanoparticles. *Chemical Society Reviews* **2015,** *44* (14), 4922-4952.
18. Cheng, X.; Ge, H.; Wei, Y.; Zhang, K.; Su, W.; Zhou, J.; Yin, L.; Zhan, Q.; Jing, S.; Huang, L., Design for Brighter Photon Upconversion Emissions via Energy Level Overlap of Lanthanide Ions. *ACS Nano* **2018,** *12* (11), 10992-10999.
19. Chakrabortty, S.; Agrawalla, B. K.; Stumper, A.; Vegi, N. M.; Fischer, S.; Reichardt, C.; Kögler, M.; Dietzek, B.; Feuring-Buske, M.; Buske, C.; Rau, S.; Weil, T., Mitochondria Targeted Protein-Ruthenium Photosensitizer for Efficient Photodynamic Applications. *Journal of the American Chemical Society* **2017,** *139* (6), 2512-2519.
20. Wang, F.; Han, Y.; Lim, C. S.; Lu, Y.; Wang, J.; Xu, J.; Chen, H.; Zhang, C.; Hong, M.; Liu, X., Simultaneous phase and size control of upconversion nanocrystals through lanthanide doping. *Nature* **2010,** *463*, 1061.
21. Pramanik, S. K.; Sreedharan, S.; Singh, H.; Green, N. H.; Smythe, C.; Thomas, J. A.; Das, A., Imaging cellular trafficking processes in real time using lysosome targeted up-conversion nanoparticles. *Chemical Communications* **2017,** *53* (94), 12672-12675.
22. Shelton, A. H.; Sazanovich, I. V.; Weinstein, J. A.; Ward, M. D., Controllable three-component luminescence from a 1,8-naphthalimide/Eu(iii) complex: white light emission from a single molecule. *Chemical Communications* **2012,** *48* (22), 2749-2751.
23. Jana, A.; Crowston, B. J.; Shewring, J. R.; McKenzie, L. K.; Bryant, H. E.; Botchway, S. W.; Ward, A. D.; Amoroso, A. J.; Baggaley, E.; Ward, M. D., Heteronuclear Ir(III)–Ln(III) Luminescent Complexes: Small-Molecule Probes for Dual Modal Imaging and Oxygen Sensing. *Inorganic Chemistry* **2016,** *55* (11), 5623-5633.
24. Sykes, D.; Cankut, A. J.; Ali, N. M.; Stephenson, A.; Spall, S. J. P.; Parker, S. C.; Weinstein, J. A.; Ward, M. D., Sensitisation of Eu(iii)- and Tb(iii)-based luminescence by Ir(iii) units in Ir/lanthanide dyads: evidence for parallel energy-transfer and electron-transfer based mechanisms. *Dalton Transactions* **2014,** *43* (17), 6414-6428.
25. De Sousa, P. L.; Livramento, J. B.; Helm, L.; Merbach, A. E.; Même, W.; Doan, B. T.; Beloeil, J. C.; Prata, M. I.; Santos, A. C.; C. Geraldes, C. F., In vivo MRI assessment of a novel GdIII-based contrast agent designed for high magnetic field applications. *Contrast media & molecular imaging* **2008,** *3* (2), 78-85.
26. Hagberg, G. E.; Scheffler, K., Effect of r1 and r2 relaxivity of gadolinium-based contrast agents on the T1-weighted MR signal at increasing magnetic field strengths. *Contrast media & molecular imaging* **2013,** *8* (6), 456-465.
27. Lee, M.-J.; Kim, M.-J.; Yoon, C.-S.; Song, S. Y.; Park, K.; Kim, W. S., The T2-shortening effect of gadolinium and the optimal conditions for maximizing the CNR for evaluating the biliary system: a phantom study. *Korean journal of radiology* **2011,** *12* (3), 358-364.